ACS APPLIED MATERIALS & INTERFACES

RESEARCH ARTICLE

www.acsami.org

Enhanced Interfacial Adhesion between an Amorphous Polymer (Polystyrene) and a Semicrystalline Polymer [a Polyamide (Nylon 6)]

Sehyun Kim,[†,‡] Jiseok Lee,[†] Hoyun Kim,[†] Youngwook P. Seo,[†] Soon Man Hong,[§] Atsushi Takahara,[⊥] Hyoung Jin Choi,[*,¶] and Yongsok Seo[*,†]

[†]Intellectual Textile System Research Center and School of Materials Science and Engineering, College of Engineering, Seoul National University, Shillim-dong 56-1, Kwanakgu, Seoul, Republic of Korea 151-744

[‡]Polymer Processing Technology Team, LG Chemical Ltd./Tech Center, Moonjidong 104-1, Yousungku, Daejon, Korea 305-738

[§]Hybrid Materials Research Center, Korea Institute of Science and Technology, Seoul, Korea 130-650

[⊥]Institute for Materials Chemistry and Engineering, Kyushu University, 744 Motooka, Nishiku, Fukuoka, Japan 819-0395

[¶]Department of Polymer Science and Technology, Inha University, Yonghyun-dong, Namku, Inchon, Republic of Korea 402-751

ABSTRACT: We studied enhanced interfacial adhesion between an amorphous polymer (polystyrene, PS) and a semicrystalline polymer (a polyamide, Ny6). The fracture mechanism for this system was investigated to elicit a universal description on the fracture mechanism. The surface modification of PS to provide functional groups that can react with the functional groups of Ny6 was carried out with ion-beam and/or plasma treatment. These surface modifications were found to alter the interfacial adhesion strength between PS and Ny6. A remarkable enhancement was found with the surface functionalization of PS. Though the fracture toughness was varied depending on the process, its overall behavior was quite similar to that of others; the fracture toughness increased with increasing bonding temperature and bonding time, passed through a peak, and then decreased with a further increase of the bonding time or temperature. The variation of the fracture toughness with the bonding time and temperature can be plausibly explained in terms of two different failure mechanisms of adhesive failure and cohesive failure. This change appears more evidently for the interface between an amorphous polymer and a semicrystalline polymer than the interface between semicrystalline polymer pairs. Surface functionalization could exclude the effect of diffusion, thus clarifying the failure mechanisms occurring at the interface.

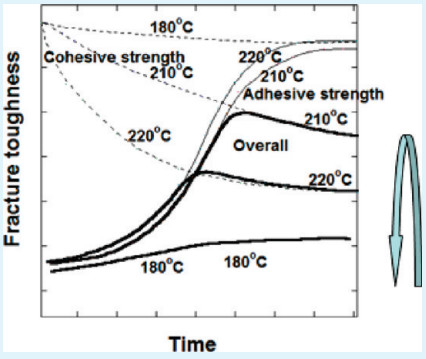

KEYWORDS: interfacial reaction, in situ compatiblization, fracture mechanisms, semicrystalline−amorphous polymer interface, chain diffusion

INTRODUCTION

Recent reports from our laboratory have dealt with the interfacial adhesion between incompatible polymer pairs.[1−6] These studies are intended, in part, to contribute to a general understanding of fracture mechanisms occurring at the interface between incompatible polymer pairs, so prevalent in polymer blends or composite systems for a lamination or coatings. Among the systems considered thus far are a semicrystalline−semicrystalline polymer pair,[5] a flexible semicrytsalline−rodlike polymer pair,[1] and an amorphous−semicrystalline polymer pair.[6] In addition to the compatibilizer effect on the adhesion between polymer pairs, we have reported the effect of surface functionalization on the interfacial adhesion to exclude the compatibilizer's diffusion problem to the interface.[4,5] All of our experimental data thus far coincided showing the same trends of the fracture toughness change with the bonding time and temperature. As long as the compatibilizer molecular weight is sufficiently large enough to form entanglements between the matrix polymers and the compatibilizers, common features of the fracture mechanisms depending on the bonding conditions can be outlined that are independent of the crystallinity of the polymer.[6] In the course of these investigations, the failure mechanism variation with the bonding time and temperature has been proposed.[1,6]

The mechanical role of a compatibilizing copolymer at the interface between two glassy polymers is now relatively well understood.[7−15] As long as the copolymer's molar mass is high enough to form entanglements with both matrix polymers and the number density of the copolymer is sufficiently high, the presence of the compatibilizer at the interface provides high interfacial adhesion strength.[4,6,8,12] If the areal density of the copolymer at the interface is insufficient to sustain a crazing stress, fracture occurs at the interface as a result of chain scission.[11,13−15] For a study of the adhesion between semicrystalline polymers, it is more complicated because they are typically two-phase materials; their deformation properties depend on the crystallization kinetics and the resulting nonequilibrium properties (cocrystallization).[15,16] We have previously investigated polypropylene (PP)/nylon 6 (Ny6) interfaces reinforced with in situ copolymer formation.[2,5]

Received: April 9, 2011
Accepted: June 20, 2011
Published: June 20, 2011

Maleic anhydride grafted PP (MAPP) was premixed with PP and then adhered to the Ny6 surface. The fracture toughness was found to increase with the bonding time, pass through a peak, and then reach a plateau. However, the high fracture toughness for a particular temperature remained yet to be explained.

In a separate study, we verified experimentally that the appearance of a maximum in the fracture toughness is not because of variation of the amount of compatibilizer formed at the interface or because of functionalized molecular diffusion to the interface.[4] To obtain these results, we used a surface functionalization method using ion-beam irradiation in an oxygen environment and produced some reactive functional groups on the PP surface at a relatively shallow depth. The fracture toughness was found to exhibit almost identical behavior: the fracture toughness passed through a maximum at 200 °C at a bonding time of 60 min.[2,4] The difference between this system and that with the compatibilizer (MAPP) was ascribed to the limited availability of functionalized molecules from the bulk. From the experimental results obtained thus far, we arrive at a conclusion that, as long as the compatibilizer's molecular weight is sufficiently large enough to form entanglements with the matrix polymers, the fracture mechanisms show a common feature, depending on the bonding times and temperature, that was independent of the polymer structure.[2,6]

To provide a better understanding, we have carried out further experiments to investigate variation of the fracture toughness between an amorphous polymer (polystyrene, PS) and a semicrystalline polymer (Ny6). In our previous study, a compatibilizer [poly(styrene-*co*-maleic anhydride), PSMA] was added for the PS and Ny6 pair.[6] We did not add a compatibilizer in this study but rather used different surface functionlization methods. We employed surface treatments consisting of Ar^+ ion-beam-irradiation and/or radio-frequency (RF) oxygen plasma treatment to exploit the necessary interfacial adhesion between PS (an amorphous polymer) and Ny6 (a semicrystalline polymer). By adopting different functionalization schemes, we tried to vary the number of surface functional groups generated on the PS surface and exclude the complexity at the interface between semicrystalline polymer pairs owing to the cocrystallization effect and the effect of the compatibilizer amount at the interface. Thus, a universal description on the fracture mechanism at the polymer—polymer interface was sought.

EXPERIMENTAL SECTION

Materials. Materials employed in this study were commercial polyamide (Ny6) and polystyrene (PS). PS was supplied by Kumho Petrochemicals (Korea). The weight-average molar mass was 2.8×10^5 g/mol, and the polydispersity index was 2.4. Ny6 was a Kolon product KN171 [37.5% crystallinity by differential scanning calorimetry (DSC) measurement; most of it was in an α form showing the characteristic peaks at $2\theta = 20°$ and 23.9°], whose weight-average molar mass was 8.5×10^4 g/mol and polydispersity index was 3.5. Pellets of all polymers were dried for 24 h in a vacuum oven at 100 °C (Ny6) and 80 °C (PS). Samples were made by compression molding at 160 and 240 °C for PS and Ny6, respectively. The PS strips (2 cm × 4 cm) were clamped with Ny6 strips (2 cm × 4 cm) in an airtight mold. The mold was heated in a temperature-controlled furnace between 180 and 220 °C. The mold was slowly cooled to room temperature in air. All of the samples were stored in a desiccator for 24 h prior to the fracture test.

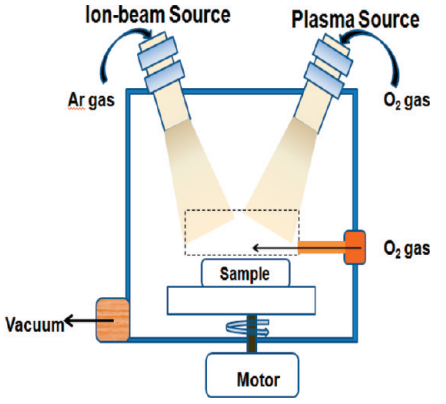

Figure 1. Schematic diagram of the ion-beam/plasma complex reactor.

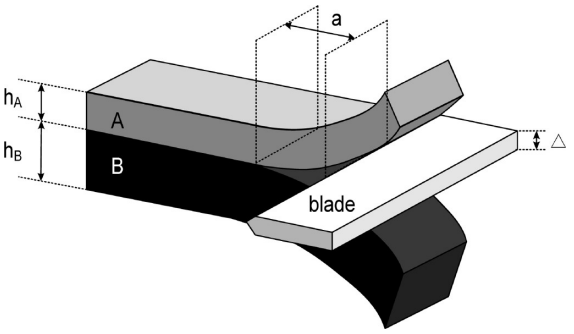

Figure 2. Schematic diagram of the ADCB test.

Ion-Beam-Irradiation and Plasma Treatment. The surface modification system consists of a low-energy ion-beam-irradiation apparatus with a reactive gas feeding system (IBO) and a conventional plasma treatment system (Figure 1). Because the reactive low-energy ion-beam-irradiation system is fully described elsewhere,[17−19] we will give a brief introduction here. It was composed of a conventional ion-beam system, a reactive gas feeding system, and a stand for the polymer samples. The flow rate of argon gas was 2 sccm, and the O_2 gas was fed with a flow rate of 5 sccm. The working pressure in the reaction chamber was kept under 10^{-4} Torr. The Ar^+ ion beam was generated from a 5 cm cold hollow cathode ion source, and its potential energy was maintained at less than 1 keV. The currents of the ions were controlled by the discharge voltage and the ion-beam potential. The discharge voltage was 400 V, and the ion fluence was varied between 5×10^{15} and 1×10^{17} ions/cm^2. The ion flux was measured with a Faraday cup placed slightly above the sample. In the oxygen plasma treatment process (OP), a RF (13.56 MHz) plasma was generated with an RF power source (RF5S-PF Power Products Inc.), and the plasma power was fixed at 100 W. The gas used in this system was O_2 with a fixed flow rate of 10 sccm. In another modification process (IBOP), the ion-beam and plasma processes were applied sequentially in the same reactor; low-energy Ar^+ ion-beam irradiation was carried out first in the absence of reactive O_2 gas to change the surface morphology, and then oxygen plasma treatment was done to functionalize the surface. The RF (13.56 MHz) plasma was again generated with the RF power source, and the plasma power was fixed at 100 W. The O_2 gas flow rate was the same as that used in the OP process.

Measurement of the Fracture Toughness. The fracture toughness was measured using the asymmetric double-cantilever beam (ADCB) test because it has been shown to be a reliable test for the fracture toughness of a polymer interface.[11−16] Details of this test are

shown in Figure 2; a blade of thickness Δ was inserted at the interface between PS and Ny6 and was pushed into the sample. Because the PS side at the experimental thickness was transparent, a video camera was used to measure the crack length exactly. An image of the region ahead of the blade was recorded after 1 h when there was no further increase in the crack length. Several images were taken on the same sample, and the same procedure was applied to different samples to get the reproducible data.

Boucher et al.[14] reported that the ADCB test yielded reliable values of the energy of adhesion, G_c, if two precautions were taken. First, the samples had to be asymmetric because different mechanical properties of the two polymers might induce various modes of fracture. They also noted that varying the ratio of thickness changed the amount of the K_{II} mode in the fracture process[14,20] and that if the fracture tended to deviate into the more ductile material, the measured energy release rate could increase significantly, leading to substantial errors in the evaluation of G_c.[10,16] To minimize contributions of the second component, all of our samples were made with a thickness ratio h_{PS}/h_{tot} of 0.67 because G_c had a minimum value at a ratio between 0.55 and 0.7.[21] In this system, Young's moduli of PS and Ny6 are 1.5 and 2.05 GPa, respectively. Because the crack length ahead of the blade, a, was less than $10h_{PS}$ for most of our samples, the following equation derived by Boucher et al.[14] based on calculations by Kanninen,[21,22] whose assumption was that the finite elasticity of the material ahead of the crack tip required correction factors for small crack lengths, was used:

$$G_c = \frac{3\Delta^2}{8a^4}\frac{E_{PS}h_{PS}{}^3E_{Ny6}h_{Ny6}{}^3}{E_{PS}h_{PS}{}^3\alpha_{Ny6}{}^2 + E_{Ny6}h_{Ny6}{}^3\alpha_{PS}{}^2} \quad (1)$$

where E_i and h_i denote Young's modulus and the thickness of material i, respectively, and Δ is the thickness of the blade. α_i is the correction factor for material i and is given by

$$\alpha_i = \frac{1 + 1.92\frac{h_i}{a} + 1.22\left(\frac{h_i}{a}\right)^2 + 0.39\left(\frac{h_i}{a}\right)^3}{1 + 0.64\frac{h_i}{a}} \quad (2)$$

Surface Morphology and Characterization. Scanning electron microscopy (SEM) observations of the samples were performed on a Hitachi S-2500C microscope. Fractured surfaces were coated with gold in an SPI sputter coater. The morphology was determined using an accelerating voltage of 15 keV. Atomic force microscopy (AFM) images were obtained using a multimode scanning probe microscope (PDS II Inc.). Noncontact mode was used to obtain height imaging data with 125-μm-long cantilevers. The lateral scan frequency was set as 1.0 Hz. The samples were moved in the $x-y$ plane, and a voltage was applied, which moved the piezoelectric driver over the z axis, in order to keep the probing force constant, resulting in a three-dimensional height image of the sample surface. Chemical components on the fractured surfaces were analyzed by X-ray photoelectron spectroscopy (XPS). The XPS spectrum was recorded by Surface Science 2803-S spectrometer ($h\nu$ = 1.5 keV). The basic pressure of 2×10^{-10} Torr was maintained during analysis. The energy resolution of 0.48 eV was maintained. The XPS spectra were referenced to the main component of the C 1s peak of PS at 284.6 eV of binding energy, the O 1s peak at 532 eV for C═O and 533.6 eV for C−O, and the N 1s peak of Ny6 at 399.7 eV. The overlapping peaks were resolved by the peak synthesis method based on a Gaussian and Lorentzian peak-fitting algorithm. Fourier transform infrared (FTIR) spectra were obtained using a Bruker 200 spectrometer (IF 66) with an average of 200 scans at a resolution of 4 cm^{-1}. Attenuated total-reflectance (ATR) adsorption spectra were recorded using an ATR accessory at a reflection angle of 30°. The crystallinity of Ny6 was analyzed using DSC, performed on a Mettler DSC 30. Prior to analysis, samples were dried at 100 °C in a vacuum oven for 24 h. About 45 mg of the dried terpolymer was used in each run. The samples were heated from 25 to 240 °C at a heating rate of 10 °C/min. The heat of fusion in the second scans was used.

RESULTS AND DISCUSSION

Surface Characterization. Figure 3 shows the surface roughness change and AFM images of the PS surfaces resulting from the different surface modification processes for various treatment times. The surface of neat PS has some large hills, mounds, and shallow valleys. The surface roughness increases rapidly with the treatment time but reaches a steady value after long irradiation time. During the ion-beam and/or plasma treatments, the PS surfaces encounter many active species. Some C−C or C−H bonds on the surface are broken during the processing, which results in the rearrangement of molecular bonds and etching on the surface and thus changes the surface morphology.[17] Some of those active species encounter those broken bonds, resulting in the implantation of polar groups onto the surface and changes in the surface chemistry.[6] The kinetic energy of the ion bombardment enhances the roughening effect rather than smoothing the etching action. Reactive O_2 gas (or oxygen plasma in the IBOP process) is then incorporated onto the surface. For the complex treatment process (IBOP), the initial roughness appears as a result of two consecutive processes (ion-beam irradiation followed by plasma treatment); hence, it reaches a steady plateau soon.[23] The etching pits, which appear at short irradiation times, evolved more fine and deeper ones with increasing irradiation time as a result of physical bombardment and chemical interaction. Because of the inherent hardness of PS, it does not show much development of the very fine needlelike morphology. All processes display similar trends showing very rough surfaces with small mountainous regions. The plasma (OP) or complex (IBOP) process produces less rough surfaces than the ion-beam-only process because of the smaller kinetic energy of plasma.

Functional groups generated on the PS surface can be checked by FTIR spectroscopy. Figure 4 shows the absorbance spectra versus wavenumber. New peaks not existing in the neat PS surfaces are observable at 1140, 1270, and 1720 cm^{-1} corresponding to the C−O symmetric stretching mode, C−O antisymmetric stretching mode, and C═O stretching mode, respectively. They can be also checked by XPS. The C 1s peak of neat PS in the XPS analysis shown in Figure 5a is symmetric with a narrow full width at half-maximum. In contrast, the C 1s peaks of the Ar^+ ion-beam-irradiated and oxygen plasma (IBOP)-treated PS sample overlap, are reduced in intensity, and are asymmetric because of the oxygen-containing groups incorporated into the surface (Figure 5b). This spectrum was decomposed into four peaks by using a Gaussian and Lorentzian peak-fitting algorithm: a C−H or C−C peak at 285.0 eV, a C−O peak at 286.5 eV, a C═O peak at 287.9 eV, and a COO peak at 289.0 eV. Table 1 shows variation of the O/C atomic ratio of surface-modified PS with the treatment time for different processes. For all three processes, the O/C atomic ratio increases with the treatment time. After more than 5 min of plasma treatment, the O/C atomic ratio, however, reaches almost a steady value except the IBO case (Figure 6), which can be explained in terms of carbonization of the PS surface and the re-etching effect: increasing the bombardment of the PS surface can result in not only cross-linking between polymer chains but also re-etching of the functionalized surface.[23] IBOP (5 min) results in the highest O/C ratio, while

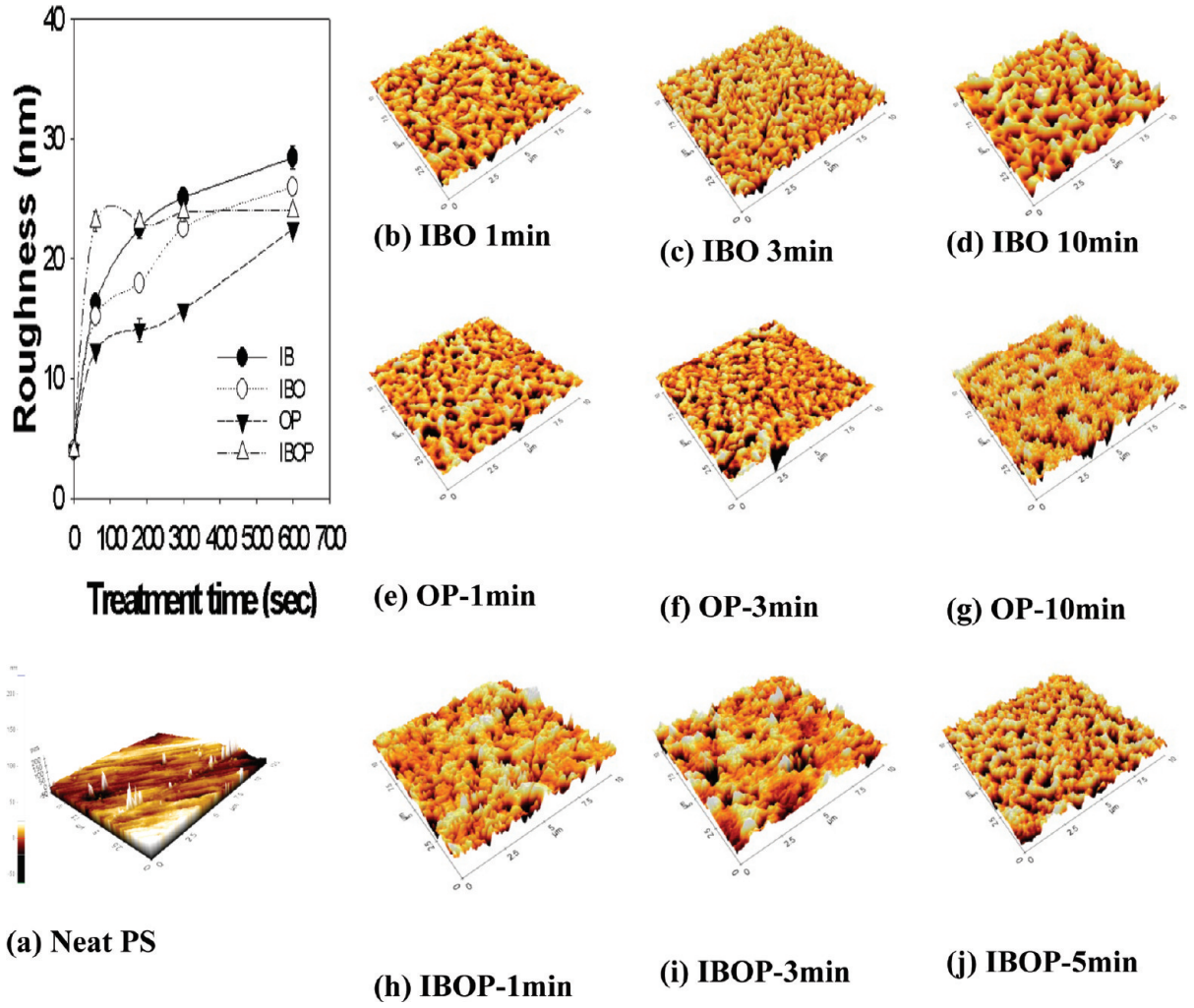

Figure 3. Surface roughness change with the irradiation time. AFM images of the modified PS surfaces.

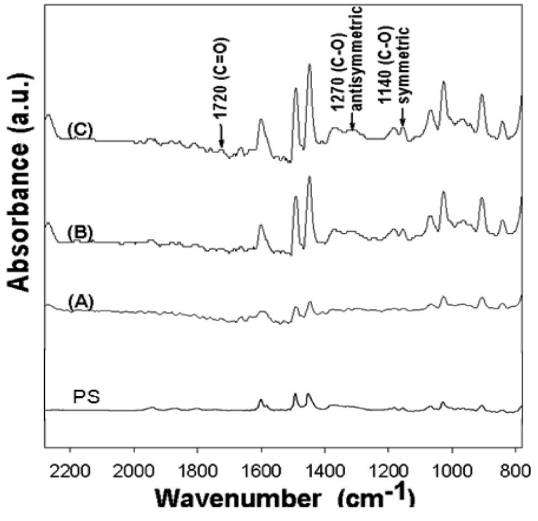

Figure 4. ATR FTIR spectra of modified PS surfaces: (A) IBO (ion-beam irradiation with reactive O_2 gas); (B) OP (oxygen plasma treatment); (C) IBOP (ion-beam irradiation plus oxygen plasma treatment).

IBO results in the lowest O/C ratio. In the IBOP process, the effect of plasma treatment becomes more significant than the OP process because of increased surface area and radical generation by previous ion-beam irradiation. On the other hand, the oxygen plasma treatment is less efficient to increase the surface area than ion-beam irradiation of higher kinetic energy. The change in the roughness during the plasma treatment process (OP) is also small because of its relatively low kinetic energy, while the effect of surface functionalization was good because of the electrically high potential, which generates bonds with the polymer chains on the surface.[17,18]

The broken bonds on the PS surface and the active oxygen species generated by the collision between the Ar^+ ion beam and O_2 gas or by the oxygen plasma encounter with each other, resulting in the implantation of polar groups onto the surface and changes in the surface chemistry. The formation of these polar oxygen-containing groups on the PS surface such as hydroxyl, carbonyl, and carboxyl groups contributes to the formation of a hydrophilic surface. This can be confirmed by contact-angle measurements. Changes in the functional-group concentrations on the PS film's surface lead to an increase of the surface free energy. The effect of irradiation on the surface polarity is shown in Figure 7. After surface treatment, the contact angle between water droplets and modified PS surfaces decreased with the irradiation time because of the effect of hydrophilicity. The PS

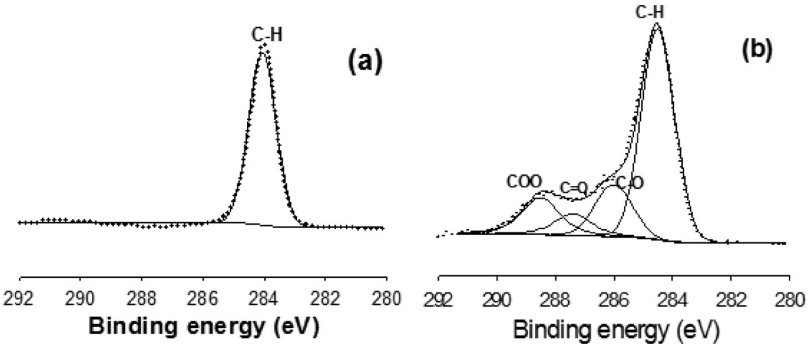

Figure 5. XPS spectra of (a) neat PS and (b) surface-modified PS (IBOP, 5 min).

Table 1. Relative Concentrations of the C 1s Components of Surface-Modified PS

		relative percentage of C 1s peak area (%)			
	treatment time (s)	C−H	C−O	C═O	COO
Ar^+ ion beam	60	79.20	9.42	8.09	3.29
+ O_2 gas (IBO)	120	75.60	11.23	7.98	5.19
	180	71.96	15.85	5.02	7.17
	300	72.00	16.56	3.44	8.00
	600	78.77	10.32	2.54	8.37
O_2 plasma only (OP)	60	66.92	13.90	9.88	9.30
	120	60.39	16.60	8.53	14.48
	180	59.31	14.73	6.76	19.20
	300	54.64	16.54	9.84	18.98
	600	54.70	16.53	12.11	16.66
Ar^+ ion beam	60	69.35	12.88	4.40	13.37
+ O_2 plasma (IBOP)	120	65.74	14.56	6.62	13.08
	180	63.79	14.70	6.58	14.93
	300	54.74	19.62	6.93	18.70
	600	54.23	18.95	8.52	18.30

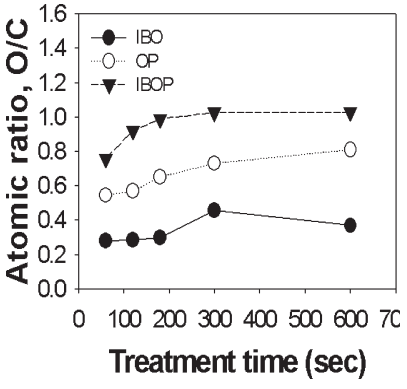

Figure 6. O/C atomic ratio of surface-modified PS with the treatment time.

film surfaces treated with plasma after Ar^+ ion-beam irradiation (IBOP) and plasma only treatment process (OP) showed lower contact angles than those treated with Ar^+ ion-beam irradiation under a reactive oxygen environment (IBO). Those two processes showed similar contact-angle decreases because of similar

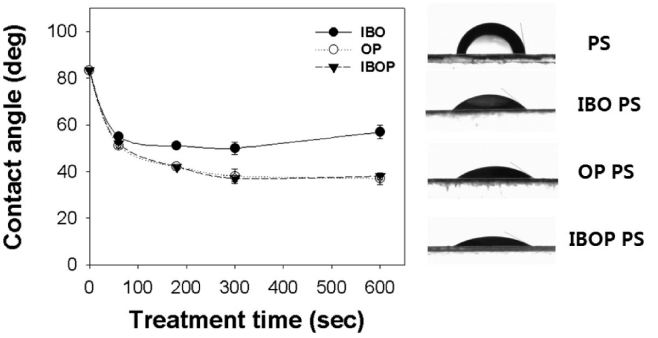

Figure 7. Variation of the contact angle with the irradiation time: IBO (●); OP (○); IBOP (▼).

O/C ratios. For the IBO case, the contact angle increased after a long irradiation time because of surface carbonization.

Fracture Toughness Variation and Fracture Mechanism. In our previous study, we found that input of functional groups on the nonpolar PP surface enhanced its adhesion with Ny6 because of the interaction between those on the PP surface and amine groups of Ny6.[4] Similarly, we expect that adhesion between the PS and Ny6 films can be significantly enhanced by generation of the polar groups on the PS film surface with ion-beam and/or plasma treatment. The strength of the adhesive joint between the PS and Ny6 films was found to vary with the treatment time (Figure 8). Up to a bonding time of 30 min, the fracture toughness increases very slowly, which indicates that not much reaction occurs at the interface; hence, some induction bonding time is required. For longer bonding times, the fracture toughness passes through a maximum and/or reaches a plateau value depending on the bonding temperature. Regardless of the surface treatment process, the peel strength is severely affected by the changes in the functional groups. Untreated PS shows a very low interfacial strength under 0.1 N/cm, whereas the interfacial strength rapidly increases with the treatment time for all of the surface modification processes. This result indicates that interaction between the functional groups on the PS surface and Ny6 is the primary reason for the adhesion improvement. The general behavior was similar to that for the interface between PS and Ny6 (PP/Ny6) compatibilized by PSMA in our previous study.[6] The adhesion strength increased with the bonding time, passed a peak value, and then reached a plateau for each temperature series higher than 190 °C. The fracture toughness also increased with the bonding temperature, passed a peak at around 200 °C, and then decreased with increasing bonding temperature.

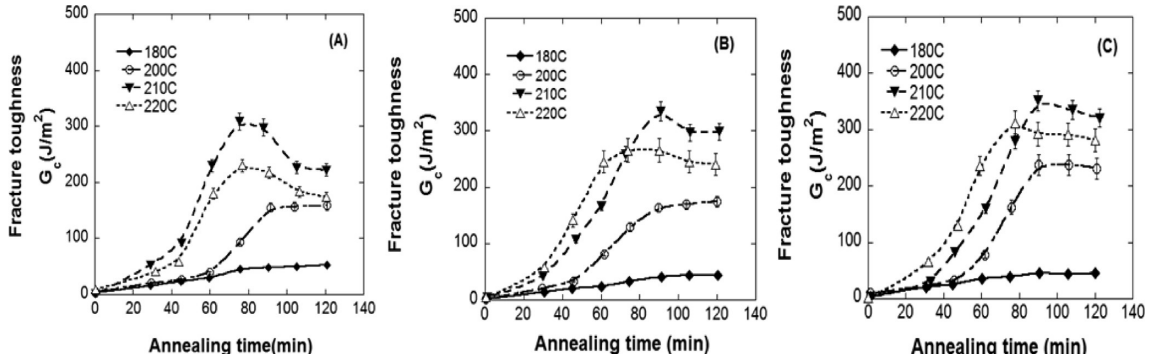

Figure 8. Variation of the fracture toughness of PS/Ny6 interface with the bonding time: (A) IBO; (B) OP; (C) IBOP.

The SEM image in Figure 9 of a fractured PS side surface shows that it contains roughened and rugged surfaces due to strong adhesion at the interface.[18,19] The irregular surface morphology was developed with the bonding time, which implies that more interactions (reactions) happened with the bonding time. This is consistent with the amount of functional groups generated on the PS surfaces (Table 1).

The fracture toughness at the same bonding time increases with the bonding temperature, reaching its highest value at 210 °C, and then decreases with further increases in the temperature (Figure 10). Also, a maximum in the fracture toughness at a bonding time of around 90 min for all bonding temperatures appears regardless of the surface treatment process. Because the cooling conditions for all of the samples were the same, the early increase in the interfacial adhesion with the bonding time is mainly due to an increase in the number of intermolecular reactions at the interface. These results are very similar to those for reactive interfacial adhesion between semicrystalline polymers (PP/Ny6),[2,4] a semicrystalline polymer (MAPP) and a thermotropic liquid-crystalline polymer,[1] and the compatibilized PS/Ny6 system in our previous study.[6] The fracture toughness increases with the areal density of the graft copolymers. As the intermolecular reactions between the functionalized PS and Ny6 molecules proceed, the interface becomes overcrowded with the graft copolymers generated at the interface. The areal density of the produced copolymers at the surface cannot be increased continuously because diffusion of functional molecules from the bulk to the interface is quite limited because of the shallow depth of functionalization.[4,5] This is different from the compatibilized system of PS/Ny6.[6] In the present PS/Ny6 system, the amine end groups of Ny6 and the functional groups easily react with each other to form covalent bonds during processing. The interface is then occupied by graft copolymers with grafting branches that are entangled with Ny6 molecules in the bulk and participate in the cocrystallization of Ny6 molecules. As long as the copolymers (or the block copolymers added as a compatibilizer) at the interface have sufficiently high molecular weights to become fully entangled with the matrix polymers on both sides of the interface, fracture occurs by chain scission when the areal density of the copolymers at the interface is low.[11,15] If the areal density of a long compatibilizer is above some critical value, the adhesive strength is high enough to withstand the fracture stress. The fracture is then determined by the cohesive strength of the polymers on either side, depending on the states of the individual chains. Thus, the failure at the interface proceeds by the mechanism with the lower intrinsic failure energy.

The temperature dependence can be plausibly explained as follows. At a low temperature of 180 °C, the reaction proceeds slowly. The concentration of grafted copolymers produced at the interface is not sufficient to produce a strong interface. The production rate increased with temperature until 210 °C. The fracture toughness showed a clear maximum at around 210 °C and then decreased at higher bonding temperatures (Figure 10). Other neat PS molecules try to escape from the highly energetic interface to the deep side of the PS matrix. This diffusion occurs more with higher temperature, resulting in less entanglements with the graft copolymers at the interface. Then the fracture will proceed inside the PS matrix rather than the interface. As a result, the entanglement of a functionalized PS molecule with other PS molecules then decreases with temperature in spite of many copolymers at the interface, and the fracture toughness decreases because of a decrease of the cohesive strength. This is also similar to the time dependence of the compatibilized PS/Ny6 system in our previous study.[6]

The time dependence of the fracture toughness can be similarly explained as follows. The initial increase in the fracture toughness with the bonding time is obviously due to an increased number of reactions. Because of entanglement with other Ny6 and PS molecules on both sides of the interface, the adhesion strength increases with the bonding time. For longer bonding times, more reaction between the functional groups of PSMA and Ny6 can happen because the PS chains can be multifunctional. As Char and Lee[24] explained, the situation may evolve from one graft per PS chain to several grafts per chain as the reaction time proceeds, hence greatly reducing the molecular weight of the PS chain portion between grafting sites that are able to entangle with other PS homopolymer molecules. As a result, the molecular weight of the "effective brush" (chain length between the brush points) at the interface decreased. The cohesive strength then decreases with the bonding time, and this occurs more rapidly at a higher bonding temperature. The overall fracture toughness increases initially with the bonding time because of the increased adhesive strength. For the case of long reaction times, the adhesive strength increases above the value of the cohesive strength, which decreases with the reaction time because of fewer entanglements. Hence, there is a maximum in the variation of the fracture toughness with time.

This outcome is summarized in Figure 11.[6] The fracture toughness at first increased with the bonding time because of the increased adhesive strength due to interfacial reactions. When the adhesive strength is lower than the cohesive strength, the failure occurs first through adhesive failure. Once the

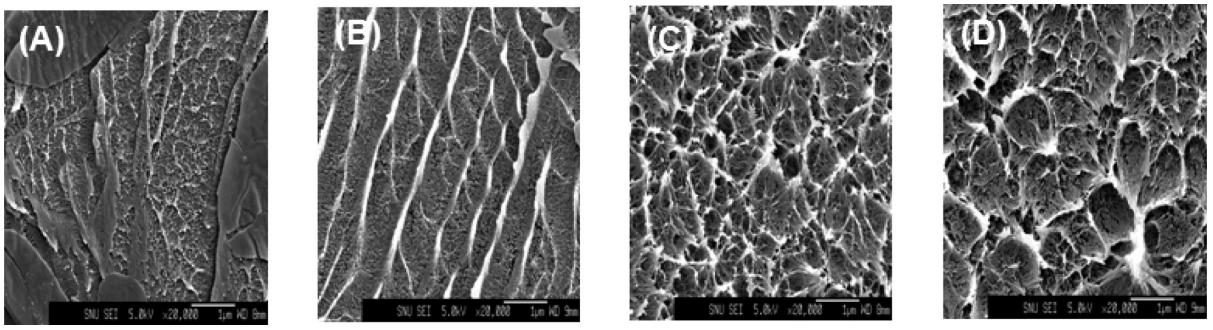

Figure 9. SEM photographs of the cleaved PS surfaces at a bonding temperature of 210 °C for 90 min of bonding time (22 000× magnification): (a) PS; (b) IBO PS; (c) OP PS; (d) IBOP PS.

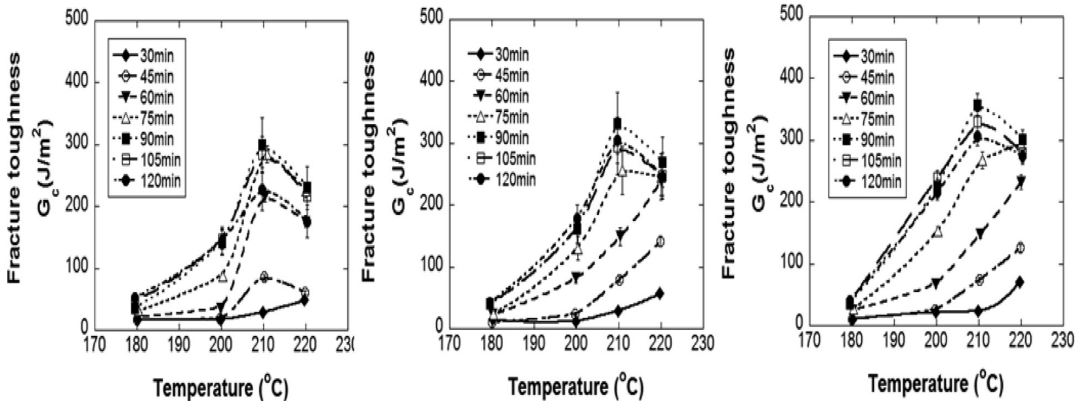

Figure 10. Variation of the fracture toughness in the PS/Ny6 interface with the bonding temperature: (A) IBO; (B) OP; (C) IBOP.

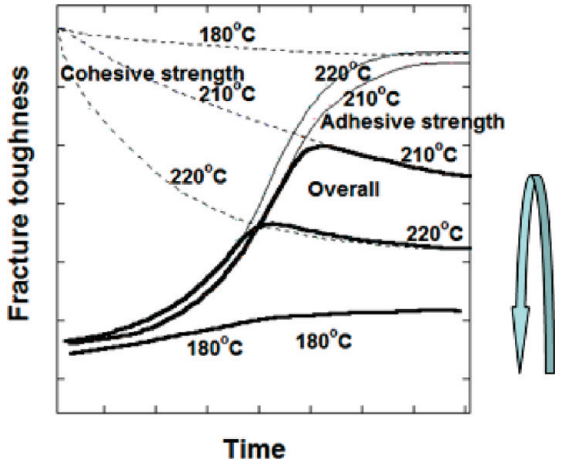

Figure 11. Schematic representation of the locus of failure of the PS/Ny6 interface. When the adhesive strength (—) is lower than cohesive strength (- - -), the failure occurs first through adhesive failure. However, after the former becomes larger than the latter, the failure occurs through cohesive failure.[6] Bold lines implicate the overall path of the failure with time at different temperatures. The arrow indicates the fracture toughness variation with the bonding temperature after some time (such as 120 min).

cohesive strength becomes lower than the adhesive strength, cohesive failure occurs.[6] This can be further corroborated by the experimental results that fracture behaviors show similar patterns for all three differently modified PS samples in spite of different amounts of surface functional groups. If the fracture strength is plotted versus the bonding time, whether a maximum appears or

Table 2. Elemental Compositions of Fractured PS and Ny6 Surfaces Measured by XPS

	PS	Ny6	
	% O	% N	% O
Bonding Time, min (IBOP Process, at a Constant Bonding Temperature of 210 °C)			
30	10.12	8.16	9.95
60	5.88	5.73	6.47
90	3.58	2.85	3.53
120	3.94	3.04	5.87
Bonding Temperature, °C (IBOP Process, at a Constant Bonding Time of 90 min)			
180	8.93	7.49	8.13
200	5.41	4.88	5.21
210	3.58	2.85	3.53
230	5.62	4.99	5.65
Three Different Surface Modification Processes (at the Optimum Conditions: 210 °C, 90 min)			
IB + O_2 (IBO)	4.24	3.69	4.02
plasma only (OP)	3.97	3.05	3.66
IB + plasma (IBOP)	3.58	2.85	3.53

not depends on the relative magnitudes of the adhesive and cohesive strengths.[1] After sufficient time, both the adhesive and cohesive strengths reach steady-state values. The temperature dependence is interpreted as follows: As the bonding temperature increases, more reactions occur faster. The adhesive strength increases more rapidly with the reaction time at high temperatures, and the cohesive strength also decreases more rapidly. Depending on the relative values of the adhesive and cohesive strengths, the total adhesion strength varies with the temperature (shown in Figure 11 by the arrow).

The elemental compositions of the fractured PS and Ny6 sides of the interface measured by XPS in Table 2 support this explanation. The key elemental difference between the PS and Ny6 sides is the presence of nitrogen in the Ny6 side. In all of the tested fractured joints, we found no nitrogen on the PS side. The crack propagates into the PS phase because of very strong adhesion at the interface, thereby leading to the disappearance of oxygen moieties. On the PS side, the disappearance of oxygen components is mainly due to the transfer of functionalized PS chains. The amount of nitrogen on the Ny6 side decreases at first with an increase of the bonding time, implying coverage of the PS molecules on this side. The amount of oxygen does not change significantly after 120 min (not listed in Table 2). For longer bonding times, the time dependence is related to the decreasing molecular weight for entanglements with other PS chains as we mentioned above. Table 2 also lists the XPS results for the samples bonded for 90 min at various temperatures. The overall behavior is similar to variation of the fracture toughness with the bonding time; it shows the change of fracture mechanisms from adhesive to cohesive fracture.

CONCLUSIONS

In this study, we attempted to elicit a universal description on the fracture mechanism at the polymer−polymer interface by experimentally studying the effect of in situ reactive compatibilization on the fracture toughness of the interface between an amorphous polymer (PS) and a semicrystalline polymer (Ny6). Surface modification of PS to provide functional groups that can react with the functional groups of Ny6 was carried out with ion-beam and/or plasma treatment. In general, the behavior of this interface was found to be similar to that of the interface between semicrystalline polymers (PP/Ny6) compatibilized by MAPP[2] and to that of the interface between semicrystalline polymer (Ny6) and amorphous polymer (PS) compatibilized by PSMA.[6]

The fracture toughness was found to increase with the bonding time, pass through a maximum value, and then reach a plateau for bonding temperatures higher than 200 °C. The fracture toughness also increases with the bonding temperature, with a maximum near 210 °C, and then decreases at higher bonding temperatures. Because the modified PS polymer chains can be multifunctional, the grafting reaction depends on the bonding temperature and bonding time. The time dependence of the fracture strength could be plausibly explained by the evolution of reacting molecules from one graft per PS chain to several grafts per chains, reducing greatly the molecular weight of the PSMA chain portion (loop or chain end) able to entangle with the other PS molecules. Thus, the molecular weight of the "effective brush" at the interface decreases. Increasing grafting density increases the adhesive strength but decreases the brush molecular weight and cohesive strength. Variation of the fracture toughness with the bonding temperature could be explained similarly in terms of two different failure mechanisms, i.e., adhesive failure at the interface for low bonding temperature and cohesive failure between the chains at the interface and the bulk of the lower modulus polymer (PS) at high temperature due to decreased chain entanglements. Therefore, there is an optimum bonding time and temperature for the fracture toughness, which appears as a maximum in variation of the fracture toughness with the bonding time and temperature. This behavior is more obvious for an amorphous polymer/semicrystalline polymer pair than for semicrystalline polymer pairs because of the absence of cocrystallization in the amorphous polymer phase.[6,12]

AUTHOR INFORMATION

Corresponding Author

*E-mail: ysseo@snu.ac.kr. (Y.S.), hjchoi@inha.ac.kr (H.J.C.).

ACKNOWLEDGMENT

This work was supported by NRF [RIAM NR03-09 (0417-20090027 to Y.S.) and R01-2006-000-10062-0 to H.J.C.], the SRC/ERC program (R11-2005-065 to Y.S.), Original Material Technology Program by MIKE [RIAMI-AC14-10 (0417-20100043) to S.M.H. and Y.S.], and a Grant-in-Aid of the Global COE Program "Science for Future Molecular Systems" under MEXT, Japan (to A.T.).

REFERENCES

(1) Seo, Y.; Ninh, T. H.; Hong, S. M.; Kim, S.; Kang, T. J.; Kim, H.; Kim, J. *Langmuir* **2006**, *22*, 3062.
(2) Seo, Y.; Tran, H. N. *Polymer* **2004**, *45*, 8573.
(3) Kim, H.; Seo, Y. *Langmuir* **2003**, *19*, 2696.
(4) Kim, H. J.; Lee, K.; Seo, Y.; Kwak, S.; Koh, S. *Macromolecules* **2001**, *34*, 2546.
(5) Kim, H. J.; Lee, K.; Seo, Y. *Macromolecules* **2002**, *35*, 1267.
(6) Seo, Y.; Lee, J.; Kang, T. J.; Choi, H. J.; Kim, J. *Macromolecules* **2007**, *40*, 5953.
(7) Paul, D. R., Newman, S., Eds. *Polymer Blends*; Academic Press: New York, 1978; Vol. 1.
(8) Paul, D. R., Bucknall, C. B., Eds. *Polymer Blends*; John Wiley & Sons: New York, 2000; Vols. 1 and 2.
(9) Wool, R. P. *Polymer Interfaces: Structure and Strength*; Carl Hanser Verlag: New York, 1995.
(10) Creton, C. In *Polymer Surfaces and Interfaces*; Richards, R. W., Peace, S. K., Eds.; John Wiley & Sons: Chichester, U.K., 1999.
(11) Creton, C.; Kramer, E. J.; Brown, H. R.; Hui, C. Y. *Adv. Polym. Sci.* **2002**, *156*, 53.
(12) Plummer, C. J. G.; Kausch, H. H.; Creton, C.; Kalb, F.; Léger, L. *Macromolecules* **1998**, *31*, 6164.
(13) Norton, L. J.; Smigolova, V.; Pralle, M. U.; Hubenko, A.; Dai, K. H.; Kramer, E. J.; Hahn, S.; Berglund, C.; DeKoven, B. *Macromolecules* **1995**, *28*, 1999.
(14) Boucher, E.; Folkers, J. P.; Creton, C.; Hervert, H.; Leger, L. *Macromolecules* **1997**, *30*, 2102.
(15) Cho, K.; Li, F. *Macromolecules* **1998**, *31*, 7495.
(16) Laurens, C.; Creton, C.; Leger, L. *Macromolecules* **2004**, *37*, 6814.
(17) Kim, H. J.; Lee, K.; Seo, Y. *Macromolecules* **2002**, *35*, 1267.
(18) Kim, S.; Lee, K.; Seo, Y. *Langmuir* **2002**, *18*, 6185.
(19) Kim, S.; Lee, K.; Seo, Y. *Langmuir* **2005**, *21*, 3432.
(20) Creton, C. F.; Kramer, E. J.; Hui, C. Y.; Brown, H. R. *Macromolecules* **1992**, *25*, 3075.
(21) Brown, H. R. *Macromolecules* **1991**, *24*, 2752.
(22) Kanninen, M. F. *Int. J. Fract.* **1973**, *9*, 83.
(23) Kim, G. H.; Hong, S. M.; Seo, Y. *Phys. Chem. Chem. Phys.* **2009**, *11*, 10506.
(24) Lee, Y.; Char, K. *Macromolecules* **1994**, *27*, 2605.